

Nanosheet-templated graphene oxide membranes for fast molecule separation

Zhen Lin¹, Chuan Hu¹, Qing Lin Liu¹, and Qiugen Zhang¹

¹Xiamen University

March 5, 2022

Abstract

Intercalated laminar membrane with controllable interlayer spacing (*d*-spacing) is one of the most effective membranes for fast molecule separation. In this work, we demonstrate a versatile strategy to create nanosheet-templated water channels in laminar graphene oxide (GO) membranes. The 1.2 nm-thick nickel hydroxide nanosheets as sacrificed intercalators provide a chance to control the *d*-spacing and simultaneously retain hydrophilicity. The resultant membranes have controllable channels and exhibit over 6 times higher water permeance than the unintercalated membrane. The 880 nm-thick nanosheet-templated GO (NST-GO) membrane has accurate *d*-spacing of about 1.14 nm and shows high water permeance of 120.3 L m⁻² h⁻¹ bar⁻¹ and good molecule separation property, reflecting in high rejection for larger dyes (90.1% for erythrosine b (EB)), while low rejection for smaller dyes (58.3% for methylene blue (MB)). Furthermore, this strategy of intercalating and sacrificing nanosheets has higher potential than traditional intercalation in controlling *d*-spacing of laminar membranes.

Nanosheet-templated graphene oxide membranes for fast molecule separation

Zhen Lin^{1,2}, Chuan Hu¹, Qinglin Liu¹, Qiugen Zhang^{1,*}

¹Department of Chemical and Biochemical Engineering, College of Chemistry & Chemical Engineering, Xiamen University, Xiamen 361005, China.

²Department of Applied Physics, School of Science, Aalto University, P.O. Box 15100, FI-00076 Espoo, Finland

*E-mail: qgzhang@xmu.edu.cn (Zhang); Tel: +86-592-2188072; Fax: +86-592-2184822

Abstr act

Intercalated laminar membrane with controllable interlayer spacing (*d* -spacing) is one of the most effective membranes for fast molecule separation. In this work, we demonstrate a versatile strategy to create nanosheet-templated water channels in laminar graphene oxide (GO) membranes. The 1.2 nm-thick nickel hydroxide nanosheets as sacrificed intercalators provide a chance to control the *d* -spacing and simultaneously retain hydrophilicity. The resultant membranes have controllable channels and exhibit over 6 times higher water permeance than the unintercalated membrane. The 880 nm-thick nanosheet-templated GO (NST-GO) membrane has accurate *d* -spacing of about 1.14 nm and shows high water permeance of 120.3 L m⁻² h⁻¹ bar⁻¹ and good molecule separation property, reflecting in high rejection for larger dyes (90.1% for erythrosine b (EB)), while low rejection for smaller dyes (58.3% for methylene blue (MB)). Furthermore, this strategy of intercalating and sacrificing nanosheets has higher potential than traditional intercalation in controlling *d* -spacing of laminar membranes.

Topical Heading: Separations: Materials, Devices and Processes

Key Words: molecule separation; laminar membrane; sacrificed intercalator; nanosheet-templated membrane; d -spacing control

1. Introduction

Molecule separation membrane has attracted increasing attention over the past few decades because of its accuracy and efficiency.^{1,2} Typically, isoporous membranes have pores with uniform size which are applicable for molecule separation.^{3,4} There are many methods to prepare the isoporous membranes, such as interference lithography,⁵ breath figure,⁶ copolymer self-assembly,⁷ etc. Among them, controlling d -spacing is an effective way to prepare the isoporous membranes with laminar nanochannels, such as GO membranes, MoS₂ membranes, WS₂ membranes, etc.^{8,9} These membranes have alterable d -spacing because the two-dimensional nanosheets can be slid or intercalated.¹⁰ Therefore, it is flexible to adjust different d -spacing and make suitable laminar nanochannels of these membranes for the separation of target molecules.

The GO membranes are one of the most common membranes that have laminar structure.^{11,12} The d -spacing between two GO nanosheets is about 0.9 nm, which is smaller than most of dye molecules but much larger than water molecules.^{13,14} This means the water molecules can penetrate easily while the dye molecules are rejected effectively. As a result, the GO membranes often have excellent dye rejection. However, the GO membranes also have unsatisfactory permeance because of their narrow water channels resulting from small d -spacing.¹⁵ Therefore, one of the most effective ways to improve the water permeance without compromising rejection is increasing d -spacing but controlling at an appropriate value.

Recently, intercalating nanomaterials into the interlayers of GO nanosheets for d -spacing control has attracted broad attention.^{16,17} The most nanomaterials used are zero-dimensional spheres. For example, Chen *et al.* reported a kind of pyrrolidinium-functionalized fullerene intercalated GO membranes.¹⁸ The membranes have broadened d -spacing of about 1.46 nm, which results in the improvement of water permeance from 4 L m⁻² h⁻¹ bar⁻¹ to 34 L m⁻² h⁻¹ bar⁻¹. Another zero-dimensional sphere are ions. Chen *et al.* intercalated ions, such as K⁺, Na⁺, Ca²⁺, Li⁺ or Mg²⁺, into GO interlayers to decrease the d -spacing and fabricated the cation-controlled membranes for desalination.¹⁹ The KCl-controlled membrane shows the ion rejection of more than 99%. One-dimensional nanowires or nanotubes are sometimes considered as well. For example, Zeng *et al.* used the modified carbon nanotubes as intercalators to control the d -spacing at about 0.85 nm.²⁰ The membranes have the enhanced water permeance of 34.4 L m⁻² h⁻¹ bar⁻¹ with over 90% rejection for dyes. Different from zero-dimensional and one-dimensional nanomaterials, two-dimensional nanosheets are more facile as intercalators because of their large surface area and lamellar structure like GO nanosheets.²¹ However, they are seldom reported because only the thin and uniform nanosheets can be used for intercalation. For example, Liao *et al.* used ultrathin zwitterionic MXene nanosheets to intercalate between GO nanosheets.²² The resulting membranes have the high water permeance of 110 L m⁻² h⁻¹ bar⁻¹ and good rejection for molecules whose size is larger than 2 nm.

Although the intercalators are various, almost of them are designed remaining in the membranes. These intercalators occupy water channels, increase filtration resistance, hinder water transmission, and finally cause unnecessary loss of water permeance. Therefore, a novel way to control the d -spacing but prevent remaining of the intercalators in the membranes should be more effective to improve the permeance of GO membranes. Inorganic hydroxide nanomaterials are potential candidates. They not only regulate d -spacing by their shapes but also can be easily removed by acid dissolution.²³ That is, the d -spacing of GO membranes can be controlled accurately, and meanwhile the water channels can be even unimpeded than traditional intercalators after sacrificing the inorganic hydroxides. For example, Huang *et al.* reported nanostrands-channeled GO membranes by sacrificing copper hydroxide nanostrands as intercalators, which increases d -spacing from 0.85 nm to 0.99 nm.²⁴ The membranes have the high rejection of 99% for large molecules like tetrakis (1-methylpyridinium-4-yl) porphyrin p-toluenesulfonate (TMPyP) while low rejection of 36% for small molecules like [Fe(CN)₆]³⁻.

The Ni(OH)₂ nanosheets, prepared by a facile way in our previous work, show great potential as intercalators.^{25,26} The nanosheets are desired two-dimensional nanomaterials which have uniform thickness

and controllable size determined by aging time. For example, the size of 0.5 hour-aged Ni(OH)₂ nanosheets is about 50×50 nm² with the thickness of about 1.2 nm. Therefore, if the nanosheets are used as intercalators, the *d* -spacing of GO membranes can be easily controlled at about 1.2 nm that is a proper size for dye separation. In this paper, we demonstrate a facile strategy to construct hydrophilic laminar channels in the GO membranes for fast molecular separation *via* the templates of ultrathin Ni(OH)₂ nanosheets. As shown in Figure 1a, the 1.2 nm-thick Ni(OH)₂ nanosheets with abundant positive charges assembled on the surface of negatively-charged GO nanosheets and formed Ni(OH)₂@GO composite nanosheets, which are used to fabricate NST-GO membranes *via* filtering, reducing and template removing in turn. The Ni(OH)₂ nanosheets provide a chance to control the *d* -spacing between GO nanosheets and simultaneously retain their hydrophilicity after reducing. Amazingly, the resulting NST-GO membranes exhibit over 6 times higher water permeance than the unintercalated membrane, showing a great potential in fast molecular separation.

2. Experimental

2.1. Chemicals

The GO gel (1 wt%) was purchased from *Aladdin Co. Ltd* . Nickel nitrate hexahydrate, 2-aminoethanol, hydrazine hydrate and hydrochloric acid were purchased from *Sinopharm Chemical Reagent Co. Ltd* . The other reagents were purchased from *Aldrich Co. Ltd* . All chemicals were not purified before usage. A Millipore direct-Q system was used to produce the ultrapure water of 18.2 MΩ, which was used throughout all experiments.

2.2. Preparation of Ni(OH)₂@GO nanosheets

The 0.1 mg mL⁻¹ GO nanosheets were prepared by diluting the GO gel and then dispersed by ultrasonication. The Ni(OH)₂ nanosheets were prepared following a previous method by quickly adding 2-aminoethanol (3.0 mM) aqueous solution into an equivalent volume of Ni(NO₃)₂ (2.0 mM) aqueous solution and then aging for 0.5 h at 20 °C. The Ni(OH)₂@GO nanosheets were prepared by mixing the GO dispersion with the Ni(OH)₂ dispersion. The structure of the three kinds of nanosheets was characterized by atomic force microscope (AFM, 5500, Agilent Technologies, USA) under the tapping mode. Transmission electron microscope (TEM, JEM-2100, JEOL, Japan) was also employed to observe the inner structure. The TEM samples were prepared by dropping the nanosheets dispersion on a copper grid coated with a carbon film and drying in air. Moreover, the width distribution of the nanosheets was measured by dynamic light scattering (DLS, Autosizer 4700, Malvern, UK) at 20 °C.

2.3. Fabrication of NST-GO membranes

The reduced GO membranes were fabricated by directly filtering 5 mL GO nanosheets dispersion onto the polycarbonate substrate, followed by the hydrazine reduction. Similarly, the reduced Ni(OH)₂@GO membranes were fabricated by reduction after directly filtering Ni(OH)₂@GO nanosheets dispersion onto the polycarbonate substrate. Afterwards, the hydrochloric acid aqueous solution (pH 2, 10 mL) was filtered across the reduced Ni(OH)₂@GO membranes to dissolve Ni(OH)₂ nanosheets for forming the nanosheet-templated channels. The obtained membranes were the expected NST-GO membranes. Besides, for comparison, parts of NST-GO membranes were reduced by hydrazine to fabricate the reduced NST-GO membranes.

2.4. Membrane characterizations

The morphological structure of as-prepared membranes was observed by scanning electron microscope (SEM, S-4800, Hitachi, Japan). The samples were prepared for cross-sectional observation by freeze-fracturing the membranes in liquid nitrogen. About 2.5 nm-thick platinum layer was coated on the surface of samples before observation using a coater (JFC-1600, JEOL, Japan). The elemental composition of the samples was determined by the energy dispersion spectrum (EDS) of SEM. X-ray diffraction (XRD) spectra was acquired by XRD meter (Ultima IV, Rigaku, Japan) with a Cu-Kα source at 40 kV and 30 mA. The *d* -spacing of the membranes could be calculated from XRD spectra by

$$d = \lambda / (2 \sin \theta) \quad (1)$$

where d is d -spacing (nm), λ is wavelength ($\lambda = 0.15$ nm), θ is incidence angle (degree). Moreover, surface hydrophilicity was determined by contact angle meter (DSA30, Kruss, Germany).

2.5. Separation experiments

The pure water permeance of the membranes was measured by filtering the ultrapure water through the membranes and calculated by

$$J = V/(Apt) \quad (2)$$

where J is the permeance ($\text{L m}^{-2}\text{h}^{-1} \text{bar}^{-1}$), V is the volume of the solution through the membranes (L), A is the effective filtration area of the membranes (m^2), p is the pressure difference across the membranes (bar), and t is the filtration time (h).

Six organic dye molecules were used as probes to evaluate nanofiltration performances of the membranes, including TMPyP (M_w 1363.60), direct yellow 50 (DY, M_w 956.82), EB (M_w 897.88), congo red (CR, M_w 696.68), oil red (OR, M_w 408.50) and MB (M_w 373.89). MgSO_4 and NaCl were also used to evaluate desalination performances. 50 mL of dye solution ($10 \mu\text{g mL}^{-1}$) or salt solution (1 mg mL^{-1}) was filtered under continuous stirring. When about one third of the solution passed through the membranes, the concentration of dyes in the feed, the retentate and the permeate was measured by the ultraviolet-visible (UV-vis) absorption spectrometer (UV-1800, Shimadzu, Japan) while the concentration of salts in the feed, the retentate and the permeate was measured by the conductivity meter (CON700, Eutech, USA). The rejection was calculated by

$$R = (C_f - C_p)/C_f \times 100\% \quad (3)$$

where R is rejection (%), C_f and C_p are the concentration of solutes in the feed and the permeate (g L^{-1}), respectively.

3. Results and Discussion

3.1. Preparation of $\text{Ni}(\text{OH})_2@$ GO composite nanosheets

The ultrathin $\text{Ni}(\text{OH})_2$ nanosheets were prepared according to our previous work.^{25,26} The 2-aminoethanol (3.0 mM) aqueous solution quickly mixed with an equivalent volume of $\text{Ni}(\text{NO}_3)_2$ (2.0 mM) aqueous solution and then aged for 30 mins at 20 °C. Clearly, the formed $\text{Ni}(\text{OH})_2$ nanosheets have the thickness of about 1.2 nm, and uniform width in the range of 13 to 50 nm with the average of 25 nm (Figure S1, Supporting Information). Subsequently, the $\text{Ni}(\text{OH})_2$ nanosheets were mixed into the aqueous GO nanosheets dispersion to produce the $\text{Ni}(\text{OH})_2@$ GO composite nanosheets. The GO nanosheets have typical monolayer structure with the thickness of about 1.0 nm, as displayed by TEM and AFM (Figure 1b, Figure S2, Supporting Information). Moreover, the GO nanosheets have the uniform width that ranges from 500 to 1300 nm and fits Gauss distribution well with the average of 800 nm (Figure 1b). It is known that the GO nanosheets have many carboxyl and hydroxy on their surface, and thus often are used to adsorb positively charged chemicals due to the electrostatic interaction.²⁷ As well, the $\text{Ni}(\text{OH})_2$ nanosheets are exactly positively charged and will assemble on the GO nanosheets in their mixture, leading to the formation of $\text{Ni}(\text{OH})_2@$ GO composite nanosheets (Figure 1a).

Figure 1c shows an AFM image of $\text{Ni}(\text{OH})_2@$ GO composite nanosheets, in which the dark background is a silicon wafer and bright layers are the GO nanosheets. Clearly, there are many bright spots on the GO nanosheets, which are attributed to the adsorbed $\text{Ni}(\text{OH})_2$ nanosheets. The height of $\text{Ni}(\text{OH})_2@$ GO composite nanosheets at positions 1 and 2 was also measured on the AFM image and shown in Figure 1d. The total height of composite nanosheets is about 2.2 nm, composed of 1 nm GO and 1.2 nm $\text{Ni}(\text{OH})_2$, in which the flat “substrates” below 1 nm are GO nanosheets while the raised “peaks” over 1 nm are the $\text{Ni}(\text{OH})_2$ nanosheets adsorbed on the GO nanosheets. This result was also revealed by TEM (Figure S3a, Supporting Information). Comparing to the GO nanosheets, the $\text{Ni}(\text{OH})_2@$ GO composite nanosheets have greater width with a broader distribution and the average of 3000 nm due to assembling of $\text{Ni}(\text{OH})_2$ nanosheets on the GO nanosheets

(Figure S3b, Supporting Information). From these, the prepared $\text{Ni}(\text{OH})_2@GO$ composite nanosheets mono-dispersed in water should form the laminar membrane on the porous substrate by the conventional filtration stacking process.

3.2. Formation and nanosheet-templated channels of NST-GO membranes

Figure 1a shows the fabrication procedure for making the NST-GO membranes. Briefly, (i) the $\text{Ni}(\text{OH})_2$ nanosheet dispersion was mixed with the GO dispersion to form $\text{Ni}(\text{OH})_2@GO$ composite nanosheets. (ii) The resulting composite nanosheet dispersion was filtered to form the $\text{Ni}(\text{OH})_2@GO$ nanosheet membrane across a microfiltration filter. (iii) The $\text{Ni}(\text{OH})_2@GO$ membrane was reduced by the hydrazine reduction process.^{13,28} (iv) Finally, the NST-GO membrane was obtained by removal of $\text{Ni}(\text{OH})_2$ nanosheets using dilute hydrochloric acid solution. The membrane structure was adjusted by controlling volume of $\text{Ni}(\text{OH})_2$ nanosheet dispersion. Compared with the pure GO membrane, the $\text{Ni}(\text{OH})_2@GO$ nanosheet membrane has rougher surfaces after reduction due to the intercalation of $\text{Ni}(\text{OH})_2$ nanosheets, as shown in Figure 2a and Figure 2b. Excitingly, the formed NST-GO membrane has many wrinkles on the surfaces resulted from removal of $\text{Ni}(\text{OH})_2$ nanosheets (Figure 2c). That is, this membrane has higher surface porosity than the pure GO membrane, which are favorable to permeance of water molecules into the membranes.

Elemental composition (C, O and Ni) of GO-based membranes prepared in this work was determined by EDS. The results are showed in Figure S4a (Supporting Information). The $\text{Ni}(\text{OH})_2@GO$ membrane has three kinds of elements (C, O and Ni), in which the O content was decreased markedly after reduction and further reduced largely after removal of $\text{Ni}(\text{OH})_2$ nanosheets. Meanwhile, the Ni was disappeared completely in the NST-GO membrane. These results reveal the $\text{Ni}(\text{OH})_2$ nanosheets were dissolved successfully by acid treatment. Figure 2d and Figure 2e show cross-sectional SEM images with elemental mapping images of the reduced $\text{Ni}(\text{OH})_2@GO$ membrane before and after removal of $\text{Ni}(\text{OH})_2$ nanosheets. The prepared membranes have typical lamellar structure of GO-based membranes.^{29,30} It is found that the red spots (Ni) intersperse among blue background (C) in the mapping image, meaning that $\text{Ni}(\text{OH})_2$ nanosheets were dispersed uniformly among large GO nanosheets. After filtering the HCl solution, the red spots disappeared and replaced by black spots, which are our expected nanosheets-templated channels in the work.

XRD spectra of GO-based membranes were characterized and showed in Figure S4b (Supporting Information). The characteristic peaks are located at 9.84° , 7.11° , 7.56° and 9.06° for the reduced GO membrane, reduced $\text{Ni}(\text{OH})_2@GO$ membrane, NST-GO membrane and reduced NST-GO membrane, respectively. Accordingly, their d -spacing are 0.88, 1.21, 1.14 and 0.95 nm respectively, as listed in Figure 2f. It can be found that the d -spacing of reduced $\text{Ni}(\text{OH})_2@GO$ membrane is 1.21 nm, which is equate to the thickness of $\text{Ni}(\text{OH})_2$ nanosheets. That is, most of $\text{Ni}(\text{OH})_2$ nanosheets were mono-intercalated between two GO nanosheets. The d -spacing decreases slightly to 1.14 nm after removal of $\text{Ni}(\text{OH})_2$ nanosheets, suggesting the nanosheet-templated channels are broadened from 0.88 to 1.14 nm, contributing to improvement of water permeance. The d -spacing would be back to 0.95 nm after reduction again. This is because the unreduced regions, which had adsorbed $\text{Ni}(\text{OH})_2$ nanosheets, were reduced at this time. From above evidence, the hydrophilic nanosheet-templated channels were fabricated successfully in the GO membrane.

3.3. Microstructure and hydrophilicity of NST-GO membranes

Figure S5 (Supporting Information) shows surface SEM images of reduced GO membrane and NST-GO membrane under the low magnification. Obviously, both of them have the characteristic surface morphology of GO-based membranes.³¹ However, the later has many wrinkles appeared on its surface due to the removal of $\text{Ni}(\text{OH})_2$ nanosheets that were intercalated between GO nanosheets. That is, the membrane surface has many nanosheet-templated channels that benefit water transport into the membrane.

To study effect of content of $\text{Ni}(\text{OH})_2$ nanosheets on the membrane formation, a series of NST-GO membranes were prepared by mixing 5 mL GO dispersion and x mL $\text{Ni}(\text{OH})_2$ nanosheet dispersion (x = 0, 1, 2, 3, 4, 5, 6 and 7). Figure 3a and Figure S6 (Supporting Information) show cross-sectional SEM images of the prepared NST-GO membranes. All of the membranes have the lamellar microstructure as the most GO membranes.³² Moreover, the membrane thickness increases gradually from 0.33 to 2.06 μm with the volume of $\text{Ni}(\text{OH})_2$

nanosheet dispersion from 0 to 7 mL (Figure 3b). This suggests the d -spacing between GO nanosheets were enlarged continually with the $\text{Ni}(\text{OH})_2$ nanosheet loading. It is noted that the membrane thickness increases quickly at a low $\text{Ni}(\text{OH})_2$ nanosheet loading, slowly at appropriate loading and quickly again at high loading. This phenomenon should have the great influence on the formation of nanosheets-templated channels and will be discussed later.

In general, the GO membranes are not stable in aqueous solution and thus need further reduction for practical applications. However, excessive reduction will cause decrease of water permeance. Thus, keeping good hydrophilicity after reduction is essential for improving water permeance of GO membranes. Figure 3c and Figure S7 (Supporting Information) show static water contact angle of NST-GO membranes. It is found that contact angle is decreased with $\text{Ni}(\text{OH})_2$ volume increasing. Typically, the contact angle of reduced GO membrane is 78.4° while that of NST-GO membrane prepared from 7 mL $\text{Ni}(\text{OH})_2$ nanosheet dispersion is as low as 39.1° . This is because more $\text{Ni}(\text{OH})_2$ nanosheets adsorb on GO nanosheets and protect more areas from reduction when immersing hydrazine. Therefore, the membranes with more sacrificed $\text{Ni}(\text{OH})_2$ nanosheets have smaller contact angle, resulting in better hydrophilicity.

3.4. d -spacing control of NST-GO membranes

It has been reported that the amount of intercalator between GO layers may influence the d -spacing of GO membranes. Therefore, the d -spacing of NST-GO membranes was measured by XRD and the spectra are displayed in Figure 4a. Clearly, the characteristic peak progressively shifts from 8.00° to 6.93° , as $\text{Ni}(\text{OH})_2$ volume increases from 1 mL to 7 mL. It indicates that the d -spacing is extended from 1.07 nm to 1.25 nm after $\text{Ni}(\text{OH})_2$ intercalation, as shown in Figure 4b. Typically, the d -spacing of the NST-GO membrane prepared from 5 mL $\text{Ni}(\text{OH})_2$ nanosheet dispersion is 1.14 nm, which is 30% larger than that of reduced GO membrane (0.88 nm) but still smaller than the molecular size of most dyes (Figure S8, Supporting Information). This means improvement of the membrane permeance without sacrifice of the dye rejection.

Notably, the increase of d -spacing of NST-GO membranes in Figure 4b can be separated for three stages, indicating three forms of NST-GO membranes. As shown in Figure 4c, the three stages are named sub-saturation, saturation and over-saturation, respectively. In sub-saturation stage, when added $\text{Ni}(\text{OH})_2$ volume is below 3 mL, GO nanosheets begin to be intercalated in most places but it is insufficient for these $\text{Ni}(\text{OH})_2$ nanosheets to full the whole interlayer. Therefore, the d -spacing is increased continuously in the sub-saturation stage. Then, in the saturation stage, it can be found a region between $\text{Ni}(\text{OH})_2$ volume of 3 mL and 5 mL, where the d -spacing is increased slowly. In this stage, the $\text{Ni}(\text{OH})_2$ nanosheets fill up interlayers totally to replenish unfilled areas of sub-saturation stage and finally form a whole lay of $\text{Ni}(\text{OH})_2$ nanosheets. Therefore, the d -spacing in the saturation stage finally becomes at the value of the thickness of single $\text{Ni}(\text{OH})_2$ nanosheet. Afterwards, as the $\text{Ni}(\text{OH})_2$ volume continually increases, the $\text{Ni}(\text{OH})_2$ nanosheets are intercalated as multilayers instead of monolayers between two GO nanosheets, resulting in amorphous water channels and increasing the d -spacing. In this stage, the d -spacing may increase to 1.25 nm or more, which is not favor of keeping the high rejection of those small dyes. Overall, the d -spacing of NST-GO membranes can be controlled by using different volumes of $\text{Ni}(\text{OH})_2$ dispersion and the membrane prepared from 5 mL $\text{Ni}(\text{OH})_2$ dispersion is the optimal membrane for dye separation.

In retrospect of Figure 3b, it can be easily found these three stages as well. The thickness is increased rapidly as $\text{Ni}(\text{OH})_2$ volume increasing in the sub-saturation stage because of the enlarged d -spacing. Then, the thickness shows a decelerated growth in the saturation stage due to the decelerated growth of d -spacing, followed by another rapid increase in the over-saturation stage. Hence, the microstructure of NST-GO membranes is directly influenced by the d -spacing and can be also controlled by added the $\text{Ni}(\text{OH})_2$ volume indirectly.

3.5. Separation performances of NST-GO membranes

As it mentioned, the volume of $\text{Ni}(\text{OH})_2$ nanosheets dispersion used for sacrificing can control the microstructure and d -spacing of NST-GO membranes, which will further influence the separation performances of the

membranes. Therefore, DY molecules were used as probes to estimate the separation performances of different NST-GO membranes. As shown in Figure 5a, it is found that the water permeance increases dramatically from $3.8 \text{ L m}^{-2}\text{h}^{-1} \text{ bar}^{-1}$ to $49.2 \text{ L m}^{-2} \text{ h}^{-1} \text{ bar}^{-1}$ when the $\text{Ni}(\text{OH})_2$ volume increases from 0 mL to 7 mL. However, the DY rejection decreases accordingly. Notably, the decrease of rejection also shows the three stages as mentioned above. In the sub-saturation and over-saturation stages, the rejection drops obviously with the d -spacing increasing. This opposite trend is because the expanded d -spacing causes the less filtration resistance for dye molecules. However, in the saturation stage, the rejection decreases indistinctively and keeps around 94%, which is due to the relatively stable d -spacing. Typically, the DY rejection of the membrane prepared from 5 mL GO dispersion mixed with the 5 mL $\text{Ni}(\text{OH})_2$ nanosheet dispersion is 94.0% with the water permeance of $32.9 \text{ L m}^{-2} \text{ h}^{-1}\text{bar}^{-1}$, which still has over 6 times increasing than the reduced GO membrane. Figure 5b is the UV-vis absorption spectra of the retentate, feed and permeate of DY solution filtrated by the NST-GO membrane. It is clear that the concentration of retentate is higher than that of the feed, indicating few adsorption behaviors happening on the membrane.

Another effective way to improve the water permeance is decreasing membrane thickness. Therefore, keeping the volume ratio of $\text{Ni}(\text{OH})_2$ versus GO at 1.0, the total volume of raw dispersion for membrane fabrication is decreased to make the membrane thinner. The cross-section of as-prepared NST-GO membranes was observed and the thickness was measured from SEM images (Figure S9, Supporting Information). The separation performances of NST-GO membranes with different thicknesses were tested and the results are displayed in Figure 5c. It is found that the DY rejection decreases while the water permeance increases as the thickness decreases. Typically, the 880 nm-thick NST-GO membrane has not only the high water permeance of $120.3 \text{ L m}^{-2} \text{ h}^{-1} \text{ bar}^{-1}$ but also a sufficient DY rejection of 87.9%.

Furthermore, a series of organic dye molecules with different sizes (Figure S8, Supporting Information) and inorganic salts were employed to investigate nanofiltration separation of the 880 nm-thick NST-GO. The solution permeance and dye rejection were tested and the results are displayed as Figure 5d. From the UV-vis absorption spectra, all of the dyes are rejected instead of adsorption (Figure S10, Supporting Information). The membrane has the rejection of more than 90% for molecules that are larger than the d -spacing of 1.14 nm while a lower rejection for molecules that are smaller than the d -spacing. For example, the rejection for EB is as high as 90.1% due to its larger molecular size ($1.2 \times 3.1 \text{ nm}^2$), which can hardly pass the membrane channels. However, the rejection for MB is just 58.3% because the smaller MB molecules ($0.9 \times 1.6 \text{ nm}^2$) can easily pass through the channels. Moreover, the membrane has the poor rejection for both divalent salt and monovalent salt as the most GO membranes performing, which needs further improvements in the future.

4. Conclusions

In conclusion, we reported a versatile approach to prepare the highly-permeable GO membranes for fast molecule separation using the templates of $\text{Ni}(\text{OH})_2$ nanosheets. The $\text{Ni}(\text{OH})_2$ @GO composite nanosheets were prepared facilely by mixing GO nanosheets and $\text{Ni}(\text{OH})_2$ nanosheets. The membranes were fabricated by directly filtering the composite nanosheets over the porous supports, followed by reduction and acid dissolution for $\text{Ni}(\text{OH})_2$ removal. The resulting NST-GO membranes have traditional laminar structure with the increased d -spacing of about 1.14 nm, which means water channels are broadened. Meanwhile, the hydrophilicity of the membranes is preserved largely because the intercalators protect most areas on the GO from reduction. Therefore, the 880 nm-thick NST-GO shows the water permeance of high to $120.3 \text{ L m}^{-2} \text{ h}^{-1} \text{ bar}^{-1}$ with a sufficient DY rejection of 87.9%. Moreover, the as-prepared membranes have the good size selectivity in the separation of organic dyes. The newly developed strategy of intercalating and sacrificing hydroxide nanosheets shows a great potential in controlling d -spacing of laminar GO membranes.

Acknowledgments

This work is supported by the National Nature Science Foundation of China (No. 21878253 and No. 21736009), Science and Technology Planning Project of Fujian Province of China (No. 2020H0003), and Science and Technology Planning Project of Xiamen City of China (No. 3502Z20206050).

Author contributions

Zhen Lin : Conceptualization; data curation; investigation; writing-original draft; writing-review & editing.
Chuan Hu : Data curation; investigation. **Qinglin Liu** : Funding acquisition; project administration; supervision.
Qiugen Zhang : Conceptualization; funding acquisition; project administration; supervision; writing-original draft; writing-review & editing.

Data availability statement

The data that support the findings of this study are available from the corresponding author upon reasonable request.

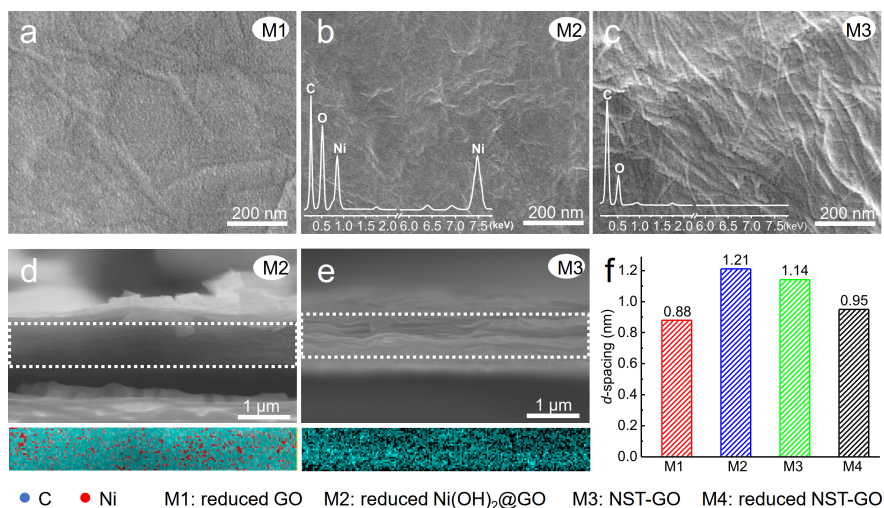
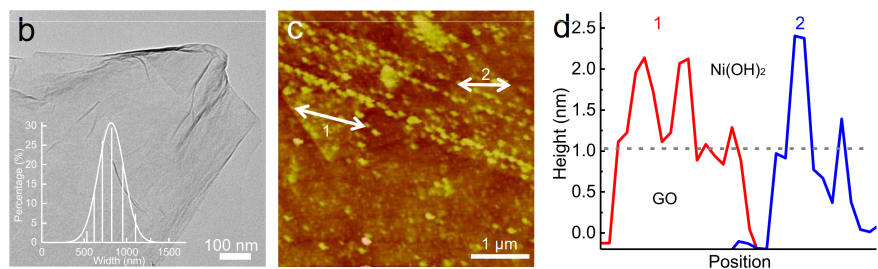
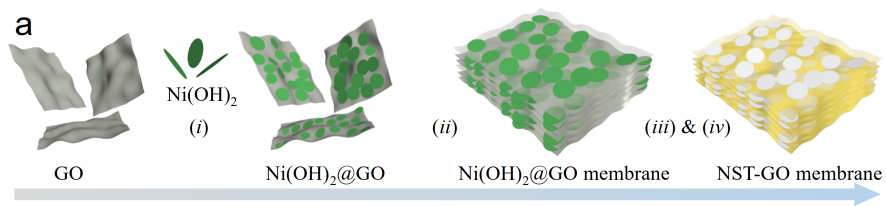
Supporting information

Additional supporting information may be found online in the Supporting Information section at the end of this article.

References

1. Wang J, Zhu J, Zhang Y, Liu J, Van der Bruggen B. Nanoscale tailor-made membranes for precise and rapid molecular sieve separation. *Nanoscale*. 2017;9(9):2942-2957.
2. Wang H, Wang M, Liang X, Yuan J, Yang H, Wang S, Ren Y, Wu H, Pan F, Jiang Z. Organic molecular sieve membranes for chemical separations. *Chem. Soc. Rev*. 2021;50(9):5468-5516.
3. Warkiani ME, Bhagat AAS, Khoo BL, Han J, Lim CT, Gong HQ, Fane AG. Isoporous micro/nanoengineered membranes. *ACS Nano*.2013;7(3):1882-1904.
4. Werber JR, Osuji CO, Elimelech M. Materials for next-generation desalination and water purification membranes. *Nat. Rev. Mater*.2016;1(5):1-15.
5. Sun M, Han K, Hu R, Liu D, Fu W, Liu W. Advances in micro/nanoporous membranes for biomedical engineering. *Adv. Healthc. Mater*.2021;10(7):2001545.
6. Tang M, Christie KSS, Hou D, Ding C, Jia X, Wang J. Fabrication of a novel underwater-superoleophobic/hydrophobic composite membrane for robust anti-oil-fouling membrane distillation by the facile breath figures templating method. *J. Membr. Sci*. 2021;617:118666.
7. Moon JD, Freeman BD, Hawker CJ, Segalman RA, Can self-assembly address the permeability/selectivity trade-offs in polymer membranes? *Macromolecules*. 2020;53(14):5649-5654.
8. Zheng S, Tu Q, Wang M, Urban JJ, Mi B. Correlating interlayer spacing and separation capability of graphene oxide membranes in organic solvents. *ACS Nano*. 2020;14(5):6013-6023.
9. Chu C, Fu C, Zhang P, Pan T, Ai X, Wu Y, Cui P, Huang Q, Ran J. Precise angstrom controlling the interlayer channel of MoS₂ membranes by cation intercalation. *J. Membr. Sci*. 2020;615:118520.
10. Wang S, Yang L, He G, Shi B, Li Y, Wu H, Zhang R, Nunes S, Jiang Z. Two-dimensional nanochannel membranes for molecular and ionic separations. *Chem. Soc. Rev*. 2020;49(4):1071-1089.
11. Zhang Y, Chung TS. Graphene oxide membranes for nanofiltration. *Curr. Opin. Chem. Eng*. 2017;16:9-15.
12. Wang Y, Liu L, Xue J, Hou J, Ding L, Wang H. Enhanced water flux through graphitic carbon nitride nanosheets membrane by incorporating polyacrylic acid. *AIChE J*. 2018;64(6):2181-2188.
13. Liang F, Liu Q, Zhao J, Guan K, Mao Y, Liu G, Gu X, Jin W. Ultrafast water-selective permeation through graphene oxide membrane with water transport promoters. *AIChE J*. 2020;66(2):e16812.
14. Liu L, Zhou Y, Xue J, Wang H. Enhanced antipressure ability through graphene oxide membrane by intercalating g-C₃N₄ nanosheets for water purification. *AIChE J*. 2019;65(10):e16699.
15. Liang F, Zheng J, He M, Mao Y, Liu G, Zhao J, Jin W. Exclusive and fast water channels in zwitterionic graphene oxide membrane for efficient water-ethanol separation. *AIChE J*. 2021;67(7):e17215.
16. Wei Y, Zhang Y, Gao X, Ma Z, Wang X, Gao C. Multilayered graphene oxide membranes for water treatment: A review. *Carbon*.2018;139:964-981.
17. Su P, Wang F, Li Z, Tang CY, Li W. Graphene oxide membranes: controlling their transport pathways. *J. Mater. Chem. A*.2020;8(31):15319-15340.

18. Chen X, Ching K, Rawal A, Lawes DJ, Tajik M, Donald WA, Zhao C, Lee SH, Ruoff RS. Stage-1 cationic C60 intercalated graphene oxide films. *Carbon*. 2021;175:131-140.
19. Chen L, Shi G, Shen J, Peng B, Zhang B, Wang Y, Bian F, Wang J, Li D, Qian Z, Xu G, Liu G, Zeng J, Zhang L, Yang Y, Zhou G, Wu M, Jin W, Li J, Fang H. Ion sieving in graphene oxide membranes via cationic control of interlayer spacing. *Nature*. 2017;550(7676):380-383.
20. Zeng W, Li C, Feng Y, Zeng S, Fu B, Zhang X. Carboxylated multi-walled carbon nanotubes (MWCNTs-COOH)-intercalated graphene oxide membranes for highly efficient treatment of organic wastewater. *J. Water Process. Eng.* 2021;40:101901.
21. Nakagawa K, Kunimatsu M, Yasui K, Yoshioka T, Shintani T, Yasui T, Kamio E, Hung W, Lee K, Tsang SCE, Matsuyama H. HNb₃O₈ nanosheet-graphene oxide composite membranes for molecular separation. *ACS Appl. Nano Mater.* 2021;4(4):3455-3466.
22. Liao F, Xu Z, Fan Z, Meng Q, Lv B, Ye X, Shen C, Zhang G. Confined assembly of ultrathin dual-functionalized Z-MXene nanosheet intercalated GO nanofilms with controlled structure for size-selective permeation. *J. Mater. Chem. A*. 2021;9(20):12236-12243.
23. Karan S, Jiang Z, Livingston AG. Sub-10 nm polyamide nanofilms with ultrafast solvent transport for molecular separation. *Science*. 2015;348(6241):1347-1351.
24. Huang H, Song Z, Wei N, Shi L, Mao Y, Ying Y, Sun L, Xu Z, Peng X. Ultrafast viscous water flow through nanostrand-channelled graphene oxide membranes. *Nat. Commun.* 2013;4(1):1-9.
25. Qu Y, Zhang QG, Soyekwo F, Gao RS, Lv RX, Lin CX, Chen MM, Zhu AM, Liu QL. Nickel hydroxide nanosheet membranes with fast water and organics transport for molecular separation. *Nanoscale*. 2016;8(43):18428-18435.
26. Lin Z, Zhang Q, Qu Y, Chen M, Soyekwo F, Lin C, Zhu A, Liu Q. LBL assembled polyelectrolyte nanofiltration membranes with tunable surface charges and high permeation by employing a nanosheet sacrificial layer. *J. Mater. Chem. A*. 2017;5(28):14819-14827.
27. Liu S, Zhou G, Guan K, Chen X, Chu Z, Liu G, Jin W. Dehydration of C₂-C₄ alcohol/water mixtures via electrostatically enhanced graphene oxide laminar membranes. *AIChE J.* 2021;67(6):aic17170.
28. Kim D, Sinha-Ray S, Park J, Lee J, Cha Y, Bae S, Ahn J, Jung YC, Kim SM, Yarin AL, Yoon SS. Self-healing reduced graphene oxide films by supersonic kinetic spraying. *Adv. Funct. Mater.* 2014;24(31):4986-4995.
29. Ali A, Aamir M, Thebo KH, Akhtar J. Laminar graphene oxide membranes towards selective ionic and molecular separations: challenges and progress. *Chem. Rec.* 2020;20(4):344-354.
30. Kang Y, Xia Y, Wang H, Zhang X. 2D laminar membranes for selective water and ion transport. *Adv. Funct. Mater.* 2019;29(29):1902014.
31. Chen D, Lin Z, Sartin MM, Huang T, Liu J, Zhang Q, Han L, Li J, Tian Z, Zhan D. Photosynergetic electrochemical synthesis of graphene oxide. *J. Am. Chem. Soc.* 2020;142(14):6516-6520.
32. Chen C, Yang Q, Yang Y, Lv W, Wen Y, Hou P, Wang M, Cheng H. Self-assembled free-standing graphite oxide membrane. *Adv. Mater.* 2009;21(29):3007-3011.



• C • Ni M1: reduced GO M2: reduced Ni(OH)₂@GO M3: NST-GO M4: reduced NST-GO

